Advances in Astronomy and Space Physics, **5**, 89-92 (2015)

Identification of the ∼3.55 keV emission line candidate objects across the sky

D. O. Savchenko[*], *D. A. Iakubovskyi*
Bogolyubov Institute of Theoretical Physics, Metrologichna str. 14-b, 03680, Kyiv, Ukraine

An emission line at the energy ∼3.55 keV detected in different galaxies and galaxy clusters has caused numerous discussions in high-energy astrophysics and particle physics communities. To reveal the origin of the line, we analyzed publicly-available observations of MOS cameras from *XMM-Newton* cosmic observatory – the instrument with the largest sensitivity for narrow faint X-ray lines – previously combined in X-ray sky maps. Because an extremely large timescale is needed for detailed analysis, we used the wavelet method instead. Extensive simulations of the central part of the Andromeda galaxy are used to check the validity of this method. The resulting list of wavelet detections now contains 235 sky regions. This list will be used in future works for more detailed spectral analysis.

Key words: X-rays: general, dark matter, line: identifications

INTRODUCTION

The new narrow emission line at ∼3.55 keV reported in February 2014 from different stacks of galaxy clusters [5], the Andromeda galaxy and the Perseus galaxy cluster [4], still remains unexplained, see reviews [12, 14] for details. Although the standard astrophysical explanation due to enhanced Kxviii emission lines at ∼3.51 keV proposed in [16] remains possible [11], subsequent measurements of the new line strength in the Galactic Centre [3, 18] and in the nearby dark matter-dominated galaxy clusters [13] argue for physics beyond the Standard Model, presumably in a form of radiatively decaying dark matter. Further studies with future high-resolution imaging spectrometers, such as Soft X-ray Spectrometer (SXS) on board forthcoming *Astro-H* mission [19] and *Micro-X* sounding rocket experiment [8] will be able to determine the line origin [5, 11, 22] in the nearest future.

Selection of the best follow-up targets is in progress. According to [2], European Cosmic Imaging Camera (EPIC) [23, 24] on board *XMM-Newton* cosmic mission [15] is the most sensitive existing instrument in order to search the narrow faint X-ray line. Recent measurement reported in [13] based on archival *XMM-Newton*/EPIC data on galaxy clusters with the largest expected decaying dark matter signal doubles the number of the new line detections compared with that in Table 1 in [14]. The result reported in [13] encourages to further search for the ∼3.55 keV line. An example of the dataset to explore is the *XMM-Newton*/EPIC sky map of [20] hat contains about 4000 individual observations (80 Ms of cleaned exposure) by the EPIC/MOS cameras of *XMM-Newton*.

Because detailed analysis of thousands of individual objects becomes an extremely challenging task, in this paper we propose the selection procedure of potential ∼3.55 keV line targets based on wavelet analysis.

METHODS

Usually, wavelets in astrophysics are used for point sources detection [6, 10, 21] and periodicity analysis [7, 9, 17], but they can also be used for search of local spectral inhomogeneities. As a simplified idea, we consider continuous spectrum with narrow line centred on bin E_i with flux F_i in i-th energy bin. By calculating flux residuals with respect to adjacent bins,

$$\Delta F_i = F_i - \frac{1}{2}\left(F_{i-1} + F_{i+1}\right),$$

we note that continuum contribution will roughly cancel while the line component localized in i-th bin will not. Sliding along the spectral range of our interest and calculating the largest ΔF_i, one can determine the line position E_0. Another important quantity – line significance S – can be estimated as

$$S(E_0) = \frac{F_i - \frac{1}{2}\left(F_{i-1} + F_{i+1}\right)}{\sqrt{F_i + \frac{1}{2}\left(F_{i-1} + F_{i+1}\right)}}. \quad (1)$$

For our analysis, we used 2 types of wavelet functions ψ:

[*] dsavchenko@bitp.kiev.ua

- step function wavelet (see Fig. 1)

$$\psi(t) = \frac{3}{2}\theta\left(t+\frac{W}{2}\right) - \frac{3}{2}\theta\left(t-\frac{W}{2}\right) - \\ -\frac{1}{2}\theta\left(t+\frac{3W}{2}\right) + \frac{1}{2}\theta\left(t-\frac{3W}{2}\right),$$

(where $\theta(t)$ is Heaviside function, W is the width of the wavelet) used in Eq. 1;

- "mexican hat" wavelet (see Fig. 2)

$$\psi(t) = \left(1-\frac{t^2}{\sigma^2}\right)\exp\left(-\frac{t^2}{2\sigma^2}\right).$$

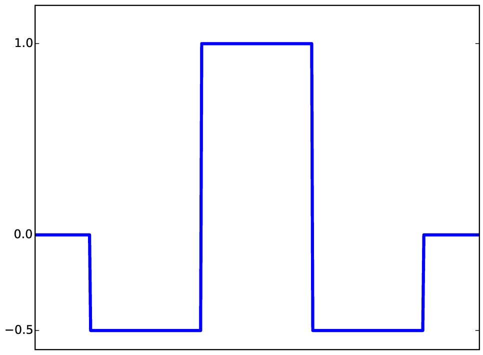

Fig. 1: Step function wavelet.

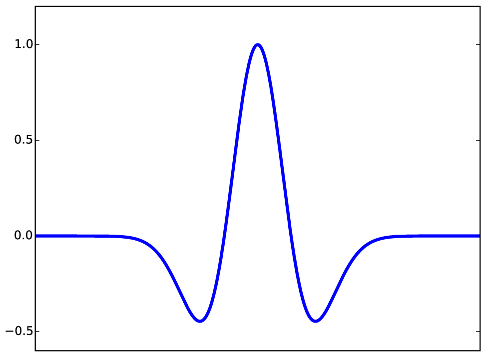

Fig. 2: "Mexican hat" wavelet.

In practice, using the wavelet method should decrease the significance of the detected line. The reasons are: the presence of non-negligible instrumental emission lines (such as Potassium Kα line at 3.31 keV and Calcium Kα line at 3.69 keV); complexes of astrophysical lines emitted by hot plasma (see e. g. Table 1 in [11]); and significant distortions of *XMM-Newton*/MOS effective area in the region of our interest. To test the sensitivity of our technique, we have simulated 5000 independent realizations of *XMM-Newton*/MOS spectra of the Andromeda galaxy where the line was already detected [4]. The simulations were performed using standard command **fakeit** inside the **Xspec** spectral fitting package. The model parameters are set equal to best-fit model parameters of real M31 spectra seen by *XMM-Newton*/MOS cameras [4]. The new emission line was included in a **fakeit** simulation model as a narrow **gaussian** model with different intensities. For each simulation, we first modelled the obtained spectrum in **Xspec** and derived the new line significance Σ using **Xspec** procedure **steppar**. For 2 extra degrees of freedom (position and flux of the narrow line) added to our model, the value of Σ and the corresponding local p-value (the probability of observing the extra line at ~3.5 keV at least as extreme as that observed in simulated spectrum, given its absence in model spectra used for simulations, see e. g. [1]) can be expressed through $\Delta\chi^2$ — the decrease of χ^2 statistics when adding a narrow **gaussian** line in **Xspec** spectral package:

$$p = \frac{2}{\sqrt{\pi}}\int\limits_0^{\Sigma/\sqrt{2}} dt\exp\left(-t^2\right) = 1 - \mathrm{e}^{-\frac{\Delta\chi^2}{2}}.$$

After that, we processed the obtained spectrum using the wavelet procedure described above and derived the largest value of our wavelet parameter S among the values of the line position E_0 within the energy range 3.45–3.60 keV[1]. To do that, we used step function wavelet with the bin width $W = 120$ eV and the "mexican hat" wavelet with $\sigma = 60$ eV. The obtained relation between the line significance Σ and the value of our wavelet parameter S for step function and "mexican hat" wavelets is plotted in Fig. 3 and Fig. 4, respectively.

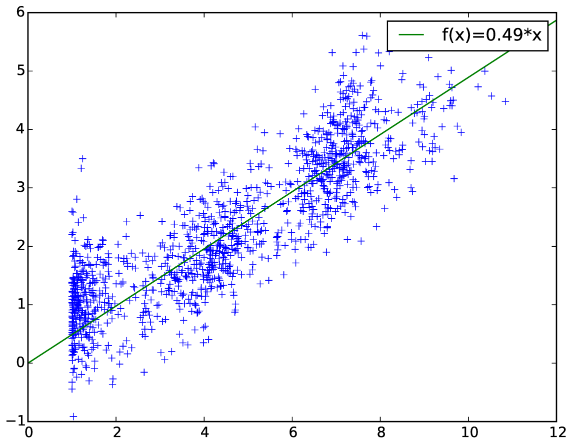

Fig. 3: Dependence of our step function wavelet significance estimator S (on Y-axis) from the local line significance Σ (on X-axis), see text. Wavelet width is set to $W = 120$ eV.

[1] By doing that, we took into account possible variations of line positions due to statistical fluctuations, see e. g. [13] for details.

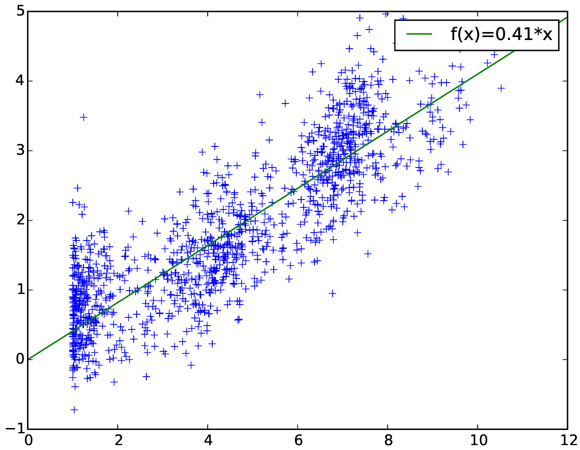

Fig. 4: The same as in Fig. 3 but for "mexican hat" wavelet with $\sigma = 60$ eV.

The resulting p-value for 3σ line detection with our step function wavelet (calculated by similar simulations with no extra line added) is 0.094 corresponding to approximately 1.7σ local significance. This means that the wavelet method, despite its simplicity, is able to recover 3σ narrow lines at 1.7σ significance. The "mexican hat" wavelet shows slightly better results (p-value is 0.082) but is much more time consuming, so for our quicklook analysis the step function wavelet is sufficient.

RESULTS AND DISCUSSION

We analyzed all *XMM-Newton*/MOS observations used in X-ray sky maps [20] in order to search the extra narrow line at $\sim 3.5\,\mathrm{keV}$[2] using step function wavelet with $W = 120$ eV described above. The format of sky maps allowed us to combine all data from the same sky regions ($25' \times 25'$ squares, roughly corresponding to *XMM-Newton*/MOS Field-of-View). We selected all the data where the new line was detected at $S > 2$ (corresponding in average to $\Sigma > 4\sigma$ local significance, according to the best-fit line in Fig. 3). The resulting list of 235 spatial regions is shown in Table 1. More detailed spectral analysis is required to reveal the presence of the line in these objects. We leave such an analysis for future work.

ACKNOWLEDGEMENT

We thank the referee, Dr. Oleksiy Agapitov, for the comments that significantly improved the quality of the paper. This work has been partially supported from the Swiss National Science Foundation grant SCOPE IZ7370-152581, the grant No. F64/42-2015 of the State Fund for Fundamental Research of Ukraine, the Program of Cosmic Research of the National Academy of Sciences of Ukraine, and the State Programme of Implementation of Grid Technology in Ukraine.

REFERENCES

[1] Babu G. J. & Feigelson E. D. 1996, *"Astrostatistics"*
[2] Boyarsky A., den Herder J., Neronov A. & Ruchayskiy O. 2007, Astroparticle Physics, 28, 303
[3] Boyarsky A., Franse J., Iakubovskyi D. & Ruchayskiy O. 2015, Phys. Rev. Lett., 115, id. 161301
[4] Boyarsky A., Ruchayskiy O., Iakubovskyi D. & Franse J. 2014, Phys. Rev. Lett., 113, id. 251301
[5] Bulbul E., Markevitch M., Foster A. et al. 2014, ApJ, 789, 13
[6] Damiani F., Maggio A., Micela G. & Sciortino S. 1997, ApJ, 483, 350
[7] Ellis J., Mavromatos N. E., Nanopoulos D. V. & Sakharov A. S. 2003, A&A, 402, 409
[8] Figueroa-Feliciano E., Anderson A. J., Castro D. et al. 2015, ApJ, 814, id. 82
[9] Foster G. 1996, AJ, 112, 1709
[10] Freeman P. E., Kashyap V., Rosner R. & Lamb D. Q. 2002, ApJS, 138, 185
[11] Iakubovskyi D. 2015, MNRAS, 453, 4097
[12] Iakubovskyi D. 2015, [arXiv:1510.00358]
[13] Iakubovskyi D., Bulbul E., Foster A. R., Savchenko D. & Sadova V. 2015, [arXiv:1508.05186]
[14] Iakubovskyi D. A. 2014, Advances in Astronomy and Space Physics, 4, 9
[15] Jansen F., Lumb D., Altieri B. et al. 2001, A&A, 365, L1
[16] Jeltema T. & Profumo S. 2015, MNRAS, 450, 2143
[17] Krivova N. A. & Solanki S. K. 2002, A&A, 394, 701
[18] Lovell M. R., Bertone G., Boyarsky A., Jenkins A. & Ruchayskiy O. 2015, MNRAS, 451, 1573
[19] Mitsuda K., Kelley R. L., Akamatsu H. et al. in *SPIE Conf. Ser.*, 9144, 2
[20] Savchenko D. O. & Iakubovskyi D. A. 2014, Advances in Astronomy and Space Physics, 4, 51
[21] Slezak E., Durret F. & Gerbal D. 1996, AJ, 108, 1996
[22] Speckhard E. G., Ng K. C. Y., Beacom J. F. & Laha R. 2015, [arXiv:1507.04744]
[23] Strüder L., Briel U., Dennerl K. et al. 2001, A&A, 365, L18
[24] Turner M. J. L., Abbey A., Arnaud M. et al. 2001, A&A, 365, L27

[2] The line position E_0 is allowed to vary within 3.45–3.60 keV range.

Table 1: List of 235 $25' \times 25'$ spatial regions with the new line at ~ 3.5 keV detected at $S > 2$ level.

S	RA	DEC	S	RA	DEC	S	RA	DEC	S	RA	DEC
3.569	255.696	33.438	3.272	141.929	−5.960	3.219	255.422	78.910	3.174	356.664	−53.796
3.174	162.793	33.770	3.060	150.368	55.633	3.056	160.302	5.934	3.041	31.042	−6.430
3.011	221.502	40.729	3.010	334.134	−17.251	2.914	318.248	13.434	2.913	159.427	53.609
2.888	98.016	−60.384	2.878	355.905	−53.423	2.863	37.253	0.620	2.852	298.943	26.153
2.833	31.458	−7.660	2.796	177.711	−28.667	2.795	283.981	1.450	2.792	237.169	27.070
2.764	217.554	42.042	2.754	331.878	10.297	2.749	296.753	34.207	2.748	160.009	39.777
2.744	278.495	−10.191	2.721	162.084	−59.971	2.717	260.130	26.500	2.715	310.385	−57.293
2.715	196.287	−40.454	2.707	70.230	25.607	2.694	187.932	25.592	2.690	24.393	−8.439
2.690	168.905	18.123	2.675	70.688	25.192	2.670	219.889	53.553	2.659	13.952	−1.039
2.650	197.542	37.054	2.633	93.722	−33.513	2.633	168.542	9.695	2.626	131.623	−50.696
2.618	66.338	15.603	2.616	186.339	32.285	2.613	282.338	0.206	2.610	202.074	−31.276
2.609	118.707	22.058	2.606	86.844	−31.890	2.604	349.648	−53.980	2.601	165.722	22.649
2.596	13.565	−73.127	2.582	265.456	−38.870	2.582	17.417	−45.779	2.577	264.565	60.097
2.576	349.659	−52.747	2.561	109.772	−24.366	2.560	25.237	−34.301	2.553	186.691	−63.914
2.533	230.877	−44.777	2.529	8.079	13.973	2.524	146.463	−8.870	2.520	318.665	13.420
2.492	154.135	−40.968	2.489	239.146	−22.034	2.474	243.486	−22.574	2.465	349.655	−53.157
2.464	210.425	−60.624	2.460	229.351	−16.047	2.457	145.877	16.837	2.444	213.247	71.493
2.443	34.367	−5.179	2.440	63.889	−59.232	2.429	267.965	23.109	2.421	125.722	22.649
2.405	276.842	6.386	2.395	167.980	43.934	2.383	85.155	35.536	2.381	55.039	−18.475
2.379	30.208	−2.290	2.378	27.689	−74.381	2.378	261.521	2.265	2.378	1.673	−34.934
2.377	73.993	−68.840	2.373	38.886	−3.905	2.369	83.329	−70.178	2.365	64.393	1.037
2.352	14.384	−26.364	2.351	147.732	−62.688	2.350	94.278	22.649	2.348	344.075	−36.316
2.348	148.905	18.123	2.336	156.019	−7.213	2.335	165.428	76.838	2.326	76.960	−70.983
2.326	225.219	1.868	2.319	350.208	8.071	2.317	70.287	−43.537	2.313	222.965	−55.847
2.309	313.772	44.304	2.306	54.337	−35.556	2.289	268.126	−6.016	2.286	231.655	51.509
2.285	103.866	−24.243	2.283	3.169	−19.662	2.280	137.884	52.896	2.278	167.710	2.704
2.274	355.503	−55.510	2.268	78.095	−67.460	2.268	263.816	−25.477	2.268	209.564	−61.457
2.267	61.609	−71.335	2.266	191.874	2.705	2.261	336.019	−1.864	2.260	354.881	−56.367
2.255	162.005	−25.390	2.253	80.212	−69.013	2.251	7.164	−77.279	2.251	357.499	36.642
2.248	191.874	8.475	2.246	181.851	28.236	2.243	348.258	−53.556	2.243	34.240	42.628
2.242	196.813	−19.248	2.231	292.013	21.446	2.228	5.219	−1.868	2.227	40.997	−48.534
2.226	188.844	26.427	2.223	216.445	42.110	2.219	154.216	−33.497	2.218	187.227	13.965
2.213	225.787	−42.213	2.212	312.121	29.276	2.208	218.470	−36.163	2.204	183.196	29.120
2.200	149.375	2.706	2.199	259.437	−59.451	2.192	25.041	−67.997	2.188	12.186	31.910
2.187	150.235	28.886	2.186	65.051	15.578	2.183	9.689	48.479	2.183	186.782	−63.085
2.180	251.169	57.704	2.175	164.393	1.451	2.169	185.633	4.354	2.168	66.108	25.143
2.167	138.074	18.371	2.160	230.799	−38.539	2.160	132.290	−2.704	2.153	258.771	−38.629
2.147	245.280	−77.252	2.144	352.413	−53.133	2.144	267.647	−37.270	2.142	283.769	15.546
2.141	254.773	−42.191	2.139	50.210	11.114	2.138	159.754	41.875	2.135	192.706	5.188
2.134	89.259	−33.156	2.134	163.171	−40.423	2.133	139.292	46.464	2.132	333.952	0.208
2.132	308.751	−33.974	2.131	68.988	−78.124	2.131	244.312	12.279	2.128	128.854	25.190
2.123	265.687	−23.892	2.121	263.285	−33.798	2.116	263.813	−33.415	2.115	20.302	−0.205
2.112	26.911	61.840	2.111	227.306	57.265	2.111	157.884	30.873	2.109	341.392	28.208
2.108	67.006	25.989	2.107	18.820	−47.323	2.102	181.945	−32.489	2.100	23.563	−36.290
2.099	291.067	13.978	2.098	136.842	0.621	2.097	8.103	39.776	2.095	39.196	61.565
2.093	179.233	52.798	2.086	86.087	−25.967	2.084	50.652	16.877	2.082	255.367	59.682
2.082	177.689	−28.263	2.082	13.019	27.220	2.080	147.337	76.449	2.079	314.896	43.847
2.079	165.122	−77.666	2.079	157.829	−34.967	2.079	140.755	30.379	2.079	122.056	−76.337
2.073	64.594	29.184	2.073	37.289	−29.498	2.070	351.883	−10.702	2.069	248.988	78.124
2.065	77.516	−69.129	2.063	220.125	64.432	2.061	14.866	−72.689	2.060	348.913	78.957
2.059	40.445	−59.862	2.057	127.269	−33.539	2.056	272.428	−19.359	2.055	195.897	−83.920
2.053	200.159	−63.615	2.050	178.886	6.761	2.049	10.208	−9.293	2.047	58.479	−0.206
2.047	179.419	26.530	2.043	34.367	−6.823	2.042	93.492	−27.619	2.042	237.051	−32.141
2.042	144.735	41.338	2.041	154.435	−58.882	2.039	89.482	−66.430	2.035	304.006	37.142
2.033	230.222	20.208	2.031	52.140	30.285	2.029	281.929	−3.091	2.027	133.227	33.527
2.027	103.129	40.837	2.025	182.005	25.390	2.021	163.093	35.850	2.018	321.130	51.185
2.016	325.166	−43.020	2.014	323.903	−54.653	2.014	243.469	−22.987	2.014	181.895	−27.427
2.009	86.957	−70.276	2.006	35.194	−4.761	2.004	267.710	−6.837	2.002	80.552	−68.144
2.002	14.723	−66.772	2.001	67.169	−17.274	2.000	83.981	−4.754			